https://doi.org/10.5194/wcd-2022-49
Preprint. Discussion started: 24 August 2022

Effects on Early Monsoon Rainfall in West Africa due to Recent Deforestation in a Convection-permitting Ensemble

Julia Crook[1], Cornelia Klein[2,3], Sonja Folwell[2], Christopher M. Taylor[2,4], Douglas J. Parker[1,5,6], Adama Bamba[7], Kouakou Kouadio[7,8]

[1] School of Earth and Environment, University of Leeds, UK
[2] UK Centre for Ecology and Hydrology, Wallingford, UK
[3] Department of Atmospheric and Cryospheric Sciences, University of Innsbruck, Austria
[4] National Centre for Earth Observation, Wallingford, UK
[5] National Centre for Atmospheric Science, University of Leeds, UK
[6] NORCE Norwegian Research Centre AS
[7] Laboratory of Material Sciences, Environment and Solar Energy (LASMES), University Felix Houphouet Boigny (UFHB), Abidjan, Cote d'Ivoire
[8] Geophysical Station of Lamto, BP 31, N'Douci, Cote d'Ivoire

Correspondence to: Julia A. Crook (j.a.crook@leeds.ac.uk)

Abstract. Tropical deforestation can have a significant effect on climate, but research attention has been directed mostly on Amazonian deforestation. The southern part of West Africa (a region dependent on rain-fed agriculture and vulnerable to droughts and flooding) has seen significant deforestation since the 1950s. Many previous tropical deforestation studies have used idealized and exaggerated deforestation scenarios and parameterized convection models. In this study we estimate realistic historical deforestation from the Land Use Harmonization dataset in West Africa and simulate the impacts in a 5-day ensemble forecast in June using a convection-permitting regional climate model. We find that sensible heat flux increases at the expense of latent heat flux in most deforested regions and rainfall increases by an average of 8.4% over deforested pixels from 18:00-6:00 UTC, whereas changes are much less pronounced during the day. Over large areas of deforestation ~300 km inland (e.g., West Guinea) the roughness-length- and thermally induced enhanced convergence during the afternoon and evening occurs over the deforested areas resulting in increases in rainfall with little impact from reduced daytime humidity. In areas of coastal deforestation (e.g., Cote d'Ivoire), increased winds drive the sea breeze convection inland, resulting in evening rainfall reductions over the deforested area but increases further inland, in line with observations. We suggest our results would not be replicated in parameterized convection models, which are known to struggle with capturing peak convective activity in the late afternoon and long-lived nocturnal rainfall, and with reproducing observed surface-rainfall feedbacks.

https://doi.org/10.5194/wcd-2022-49
Preprint. Discussion started: 24 August 2022

1 Introduction

The impact of tropical deforestation on climate has been a research area since the early 1990s but there has been particular emphasis on studying Amazonian deforestation due to the Amazon's large size (Lawrence and Vandecar, 2014; Spracklen et al., 2018). In contrast, there has been much less emphasis on West African deforestation. The impact of deforestation on rainfall is dependent on the spatial scale of land cover change, the surface flux characteristics of the replacement land cover, the nature of the rain-bearing systems, and the potential role of topographic and sea-breeze circulations, which makes it difficult to extrapolate what would happen in one region from what happens in another (Lawrence and Vandecar, 2014). There has been considerable deforestation during the 20th Century in the southern part of West Africa (Aleman et al., 2018), with pockets of deforestation driven by the rapidly growing population (Brandt et al., 2017). West Africa has experienced prolonged drought since the late 1960s, but more recently rainfall has somewhat recovered. It is likely that large scale patterns of sea surface temperatures have caused these droughts, while it has been suggested that land use change may have also had some impact (Wang et al., 2004).

Although there is consensus that tropical deforestation causes warming, the impact on rainfall is much more dependent on the spatial scale, extent, and location of the deforestation. Impacts on temperature have been determined from models and observations (Duveiller et al., 2018; Alkama & Cescatti, 2016; Perugini et al., 2017). Deforestation causes increases in albedo which cause cooling, but across the tropics this effect is more than offset by a shift in surface fluxes from latent to sensible heat, resulting in net warming of the atmosphere. The shift from latent to sensible heat flux is due to the lower leaf area index and shallower rooting; the reduction in surface roughness reduces turbulent exchange of heat from the surface, also contributing to a warmer land surface (Spracklen et al., 2018). These modifications to energy fluxes can affect rainfall. Studies of continental scale deforestation using global climate models have shown reductions in rainfall over the deforested areas, especially during drier seasons (e.g., for complete deforestation of tropical African rainforests see Werth and Avissar, 2005; Semazzi and Song, 2007). However, when more realistic deforestation scenarios were applied to the Amazon, reductions in rainfall were found to be less, and patterns of rainfall shifted, with some regions having increased rainfall (Medvigy et al., 2011). Abiodun et al. (2008) investigated two idealized but reasonably large-scale deforestation scenarios over West Africa and showed that both could have a significant impact outside the deforested area as well as locally, enhancing the monsoon flow either by changes in meridional temperature gradient (desertification scenario) or by surface roughness changes (deforestation scenario). Overall, they found a reduction in rainfall due to enhanced moisture transport out of the area. Boone et al. (2016) analyzed the impact of estimated land use/land cover change since the 1950s in West Africa in several models. Their somewhat idealized prescribed land cover change represents a worst-case degradation scenario, and they find a reduction in rainfall across the Sahel in all models and a shift in rainfall to the south in some models. Satellite observations of Rondonian (Amazonia) rainfall over deforested areas suggest an increasing rainfall trend in the dry season over the 20th century, but a decreasing trend in the wet season (Chagnon and Bras, 2005). A new observational study for Southern West Africa (Taylor et al, 2022) has identified that mesoscale deforestation locally

https://doi.org/10.5194/wcd-2022-49
Preprint. Discussion started: 24 August 2022

enhances the frequency of daytime convective activity, an effect which is particularly pronounced where coastal deforestation enhances storms triggered by sea-breezes. A positive correlation between forest minus non-forest differences in sensible heat (from flux tower measurements) and cloud cover (from satellite observations) has been found globally (Xu et al., 2022), with tropical regions typically showing increased sensible heat and cloud due to the small-scale deforestation. Differences in surface heat fluxes between clearing and adjacent forest induce mesoscale circulations similar to land-sea breezes, bringing moisture rich air from over the forest to over the clearing and, if these circulations are strong enough, result in enhanced rainfall (Souza et al., 2000; Garcia-Carreras et al., 2011; Hartley et al., 2016). Feedbacks on the atmosphere from land surface heterogeneity have been shown to be improved for high resolution convection-permitting models (CPM) compared to parameterized convection models (PM) (Taylor et al., 2013) and therefore high-resolution PM may fail to produce the observed enhanced convective rainfall at vegetation boundaries. Many of the deforestation-scenario modelling studies have used low resolution global climate models. However, mesoscale models can reproduce the deforestation-induced mesoscale circulations which have also been observed in Amazonia (D'Almeida et al, 2007). Khanna et al. (2017) used an 8km scale model to simulate Rondonian rainfall over deforested areas using 1980s and 2006 land cover. Although their 8km model can explicitly represent some of the larger scale convection their cumulus parameterization was used for smaller scale convection. Consequently, they looked at the top of boundary layer humidity as well as rainfall changes. They found the enhanced rainfall/humidity over the deforested area in the 1980s was due to thermally driven enhanced mesoscale circulations, whereas the more recent larger scale of deforestation caused enhanced rainfall/humidity only on the downwind side with roughness length changes inducing dynamically driven mesoscale circulations. CPM simulations should provide added value to representing the climate impacts of land use change (Vanden Broucke et al., 2017), because they better represent the differences in diurnal cycles of surface fluxes over different vegetation types. This is partly due to the higher resolution but largely due to representing the diurnal cycle of convection better than PM.

In this study we evaluate the changes in rainfall in a 5-day ensemble due to realistic historical deforestation (since 1950) in West Africa using a CPM and analyse the causes of the changes. We use a 5-day ensemble rather than a longer-term simulation so that we can look at how local physical processes respond to deforestation in a statistical way without diverging synoptic conditions. To our knowledge, no other studies have used a CPM or such a methodical way to determine the historical deforestation scenario to estimate effects of tropical deforestation on rainfall in this region. We analyze the diurnal cycle of various diagnostics to understand the causes of rainfall changes. We look in detail at two subregions, one where the rainfall changes are primarily thermally driven and one where the rainfall changes are primarily dynamically driven. The model and simulations are described in Section 2, the effect of deforestation on the different diagnostics are presented in Section 3, a comparison with other West African studies is presented in Section 4, and conclusions are presented in Section 5.

https://doi.org/10.5194/wcd-2022-49
Preprint. Discussion started: 24 August 2022

2 Model Setup and Methods

2.1 Modelling Strategy

We use the Met Office Unified Model (UM v8.2) with atmosphere and land surface components, run at 4 km resolution over West Africa (approximately 20° W–20° E, 0–25° N), as described in Crook et al. (2019). To assess the impact of recent West African deforestation on rainfall, we produced two 10-member 5-day ensembles, the first using current land cover and the second using an estimate of 1950's land cover. Both current and 1950 vegetation ensembles were run at 4 km resolution for 5 days from 1st June 2014 conditions over West Africa. We chose early June because at this time of year there is some rain in the region up to about 15° N, while still being early in the monsoon season when it is expected that sensitivity to deforestation is high, i.e., soils are still relatively dry, and the evaporative advantage of forests compared to shallow-rooted vegetation is expected to be high. Although earlier in the year the soil would have been drier near the coast, there were fewer rain events making detection of impacts on rainfall challenging. The ensemble approach with 10 paired members allows us to evaluate the uncertainty in the modelled response to forest cover change that is linked to internal variability. At the same time, by simulating only 5-day time slices in "forecast mode", temporal divergence of the synoptic conditions between the ensemble members is minimized. Differences between the two ensembles can therefore be attributed to the imposed deforestation in the absence of large-scale circulation feedbacks.

Sea surface temperatures and boundary conditions were prescribed from ERA-Interim data (Dee et al., 2011) every 6 hours. The ensembles were generated by starting each ensemble member from the previous current land cover ensemble member dump file at the end of the first day with the time reset to 1st June 00:00 but resetting the soil moisture to the climatology. Climatologies for soil moisture were produced as in Crook et al. (2019) from 14-year off-line land surface model (JULES) runs using either the current or 1950s vegetation.

JULES (Best et al., 2011) is a modular land surface model, handling exchange of heat, moisture and momentum with the atmosphere, soil moisture hydrology split into four soil layers of thicknesses 0.1, 0.25, 0.65, and 2.0 m, surface and sub-surface runoff parameterizations, and a vegetation model representing five different plant functional types (PFTs): Broadleaf trees (BT), needleleaf trees, C3 grass, C4 grass, and shrub. Plant and soil properties (e.g., albedo, roughness length, leaf area index (LAI), soil conductivity and soil thermal capacity) and fractions of each PFT as well as urban, ice and water per grid box are specified through ancillary files and model configuration. The amount of moisture in each soil layer available to each PFT depends on soil properties and on the root density of each PFT in each soil layer, whereas water available for evaporation from bare soil only comes from the uppermost soil layer. Due to a lack of suitable in-situ flux measurements in the study region, JULES' translation of deforestation into changes in net radiation and surface flux partitioning cannot be directly validated. However, based on known effects of tropical deforestation in better studied regions (e.g., Silvério et al., 2015 (Amazon); Peng et al, 2014 (China)), the flux differences between forested and deforested areas in the default JULES configuration did not appear sufficiently realistic, as detailed below. Such unrealistic responses to land cover change in "out-

https://doi.org/10.5194/wcd-2022-49
Preprint. Discussion started: 24 August 2022

of-the-box" land surface schemes are not unusual (Pitman et al., 2009; Boone et al., 2016). We therefore implemented the following modifications in JULES to simulate a more plausible depiction of deforestation.

2.1.1 Changes to leaf area index

Firstly, we found that the monthly climatology of LAI used in standard JULES/MetUM simulations produces an unrealistic seasonal cycle over Southern West Africa. This problem was traced to the treatment of missing data in the creation of the LAI field whereby cloudy pixels were erroneously assigned LAI of zero. Given that during boreal summer, cloud cover is extensive, the effect was to introduce a marked minimum in LAI across the region. Instead, we used an alternative LAI field (Semeena et al., 2021) based on the Global LAnd Surface Satellite (GLASS) LAI product (Xiao et al., 2016) which exhibits a broad maximum in LAI during these months (see supporting material Fig S1).

2.1.2 Changes to root water extraction for broad leaf trees

The JULES model expresses the impact of soil water stress on transpiration via a dimensionless stress factor (FSMC), based on soil moisture relative to texture-dependent critical (θc) and wilting (θw) points (Best et al., 2011, see equation 52). A value of 1 means there is no water stress at all and a value of 0 means the plant is totally water stressed. For each plant functional type, this is computed by weighting FSMC at each soil layer by its assumed vertical root profile, where the root density in each layer follows an exponential distribution with depth as given by equation 50 in Best et al. (2011).

For the BT type of key interest in our study, the root weighting for the lowest soil layer (1-3 m) is substantial, corresponding to 0.55. We found in offline simulations that throughout the first few months of the rainy season, this lowest soil level remained strongly water-stressed, suppressing the root-weighted FSMC (and hence transpiration) from trees. By contrast, shallower-rooted grasses exploit the wetter soil closer to the surface and produce much larger transpiration than the trees. We consider that in real life, trees are well adapted in terms of where they take their water from, and we hence modified JULES for BT so that FSMC is taken from the maximum value of the 4 levels, rather than its root-weighted mean.

2.1.3 Under-canopy evaporation switched off

In JULES, direct evaporation from the upper soil layer occurs primarily from the soil tile. However, soil evaporation provides an additional source to transpiration for the vegetated tiles. Under some circumstances, this is known to exaggerate the contribution of direct soil evaporation to total evapotranspiration (Van Den Hoof et al., 2013). We found that this source could (counter-intuitively) enhance evapotranspiration following deforestation and we therefore switched it off for all plant tiles.

2.2 Creation of the deforestation scenario

To identify the impact of historical deforestation on the atmosphere we require both a current and 1950s vegetation map. The current land cover is based on the European Space Agency's Land Cover Climate Change Initiative (CCI) land cover dataset,

https://doi.org/10.5194/wcd-2022-49
Preprint. Discussion started: 24 August 2022

version 1.4 for the 2008-2012 epoch (Poulter et al., 2015), which classifies each 300 m pixel as one of 23 United Nations Land Cover Classification System (UNLCCS) classes. These are mapped to the model PFTs according to Poulter et al. (2015). Creating a plausible map of vegetation in 1950 consistent with the JULES model is more challenging, and we summarize the process in Fig 1a. Firstly, we use estimates of land use change from 1950 to the present from the Land Use Harmonization (LUHv2) dataset developed for use by Earth System Models (Hurtt et al., 2011). This describes the landscape in terms of fractions of different land use types, rather than the PFTs which JULES requires. We therefore developed a mapping procedure specific to West Africa to translate land use types into fractional coverages of PFTs plus the non-vegetation functional types of inland water and bare soil fractions. For this we identified areas of primary land from the World Database of protected areas (UNEP-WCMC and IUCN, 2014). Considering only the nature reserves with the highest level of conservation (IUCN categories I to VI), we extracted the 300m CCI pixels within each protected area. Recognizing that even within these zones, there will be some degree of human disturbance, we identified the UNLCCS class with the highest fractions of BT and Shrub within each protected area. Mean annual rainfall across West Africa provides a dominant control on the composition of natural vegetation. Using the JULES composition of natural vegetation, as sampled within protected areas, we devised a simple threshold-based mapping of natural vegetation as a function of mean annual rainfall. For rainfall, we used version 2 of the CHIRPS dataset (Funk et al., 2015), downscaled to the 4 km model grid for years 1981 to 2015. The rainfall thresholds and dominant natural land cover classes (Shrub land to bare soil, Shrub land, broadleaved deciduous and broadleaved) and how they relate to model PFTs are summarized in Fig 1b. To create a map of primary vegetation cover in terms of JULES PFTs, we applied the relationships in Fig 1b to the mean annual rainfall map.

In step 2 we apply the change in primary land to produce a map of 1950 land cover, selecting all 4km model pixels within a 0.5° grid box in turn. To avoid introducing artificial 0.5° structure into the high-resolution land cover map a Gaussian-smoother is first applied to the LUHv2 map of primary land cover change. For each 4km pixel we compare ratios of existing land and primary vegetation to identify the proportion of current primary land and then apply the change to that 4km grid box fraction. In cases where the 4km values are already at or close to the primary land fractions we iteratively apply changes to the remaining pixels so that overall, the 0.5° change is applied. For the remaining non-primary land fraction, we adjust the remaining proportions of C3, C4, shrub and bare soil accordingly. Grid box urban and water fractions are kept at their 2010 values, e.g., no account taken of the construction of the Akosombo dam of the Volta River in 1965 or changes in urbanization.

https://doi.org/10.5194/wcd-2022-49
Preprint. Discussion started: 24 August 2022

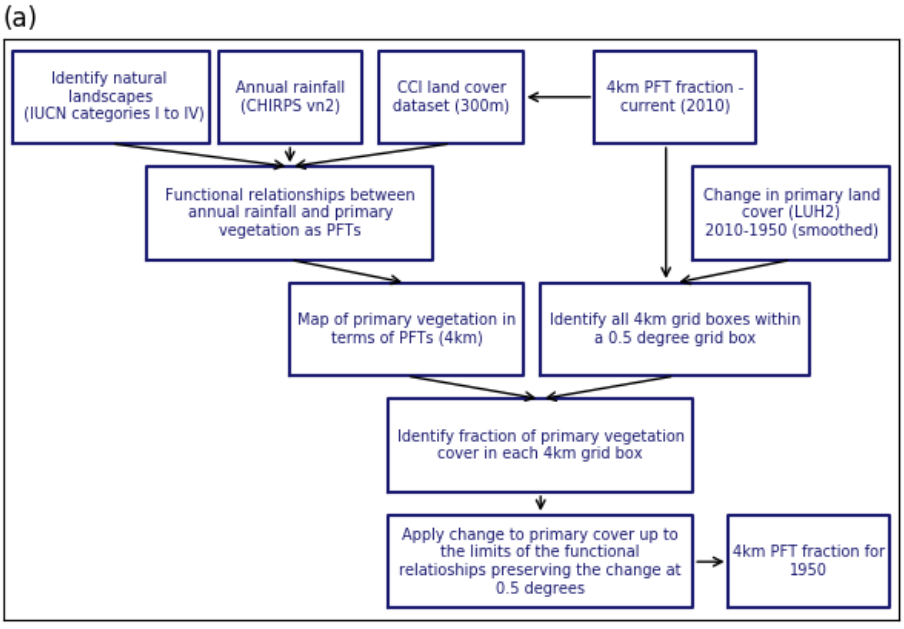

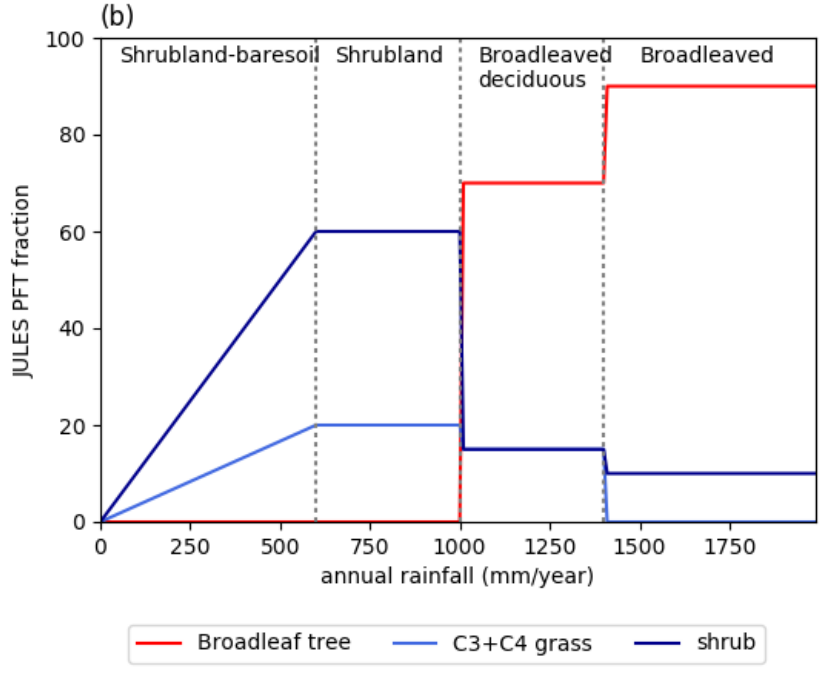

185 **Figure 1: (a) Schematic showing datasets and processing steps to produce the 1950 PFTs fractions. (b) Rainfall (CHIRPS) thresholds and the dominant "natural" UNLCCS classes identified in the CCI land cover dataset and corresponding PFT fractions identified for the West African domain.**

https://doi.org/10.5194/wcd-2022-49
Preprint. Discussion started: 24 August 2022

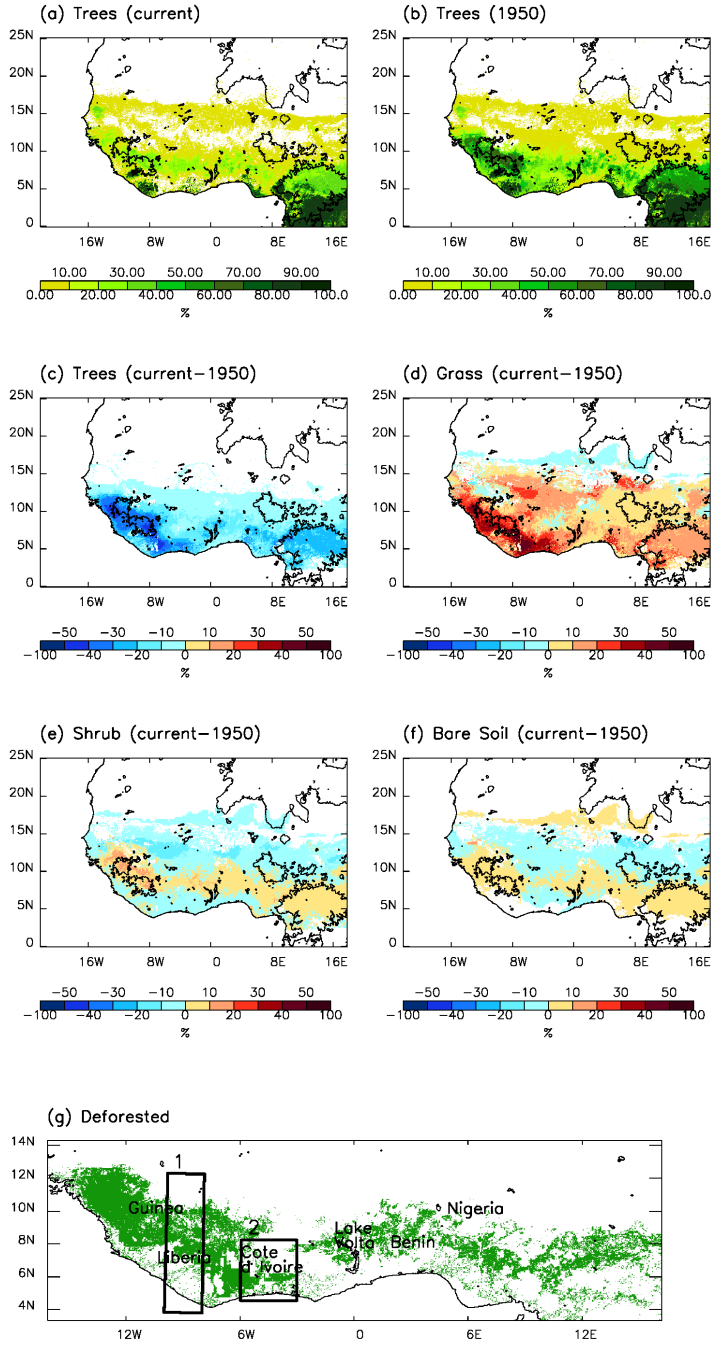

Figure 2: Tree cover for a) current and b) 1950s, differences in cover of (c) trees, (d) grass, (e) shrubs and (f) bare soil (land higher than 500m shown by black contour) and (g) deforestation mask with 2 sub-regions analyzed highlighted with black rectangles. Deforestation is defined as where 1950 tree cover > 30 %, current tree cover < 30% and change in tree cover > 10%.

https://doi.org/10.5194/wcd-2022-49
Preprint. Discussion started: 24 August 2022

Figure 2, which indicates the simulated region, shows maps of the changes in trees, grass, shrubs, and bare soil from 1950 to current. Trees have largely been replaced with grass although there have been some changes to shrubs and bare soil.

2.3 Analysis Methods

We first show the impact of the deforestation on surface characteristics of albedo, roughness length and initial soil moisture. We then compare the 5-day means (current vegetation simulations vs. 1950s vegetation simulations) of turbulent and radiative heat fluxes, 1.5m temperature, conditional instability (a proxy for convective available potential energy (CAPE)), 10m winds, and rainfall. Paired student T-tests of the 5-day means of the current and 1950's vegetation ensemble members are used to determine significant changes. In the case of rainfall, the natural logarithm of rainfall is taken first before performing the T-test because rainfall is not normally distributed. We determine significance of changes at the 95% confidence interval ($p<0.05$) for all variables except rainfall, where we relax the significance to the 90% confidence interval ($p<0.1$) due to the patchy nature of rainfall over the short duration of our simulations.

We define deforestation as where 1950 tree cover > 30 %, current tree cover < 30% and change (current-1950) in tree cover > 10% (Fig 2g). We use 30% tree cover as separating forest from non-forest as there appears to be a changeover in behaviour of turbulent fluxes around this level (supporting material Fig S2). This value was also used by Hartley et al. (2016).

We then look at two specific regions with different 1950s winds and deforestation patterns, where there have been large changes in rainfall caused by different thermal and dynamical responses.

3 Results

3.1 Albedo, Roughness length and Initial Soil Moisture

The changes in vegetation result in changes in albedo and roughness length as shown in Fig 3a and 3b, respectively. Albedo mostly increases over the deforested areas by up to 0.02 from around 0.15 (i.e., by up to ~12 %), although there are some areas with small decreases coinciding with where shrubs have increased. Roughness length decreases over the deforested area by around 0.5m compared to the 1950s, where roughness length is typically 1-3m over the forested area. In June, the monsoon has reached the southern part of the region and the soil moisture is high enough that soil moisture control on transpiration is weak (tile-weighted soil moisture stress factor (FSMC) >0.8), whereas further north it is stronger (Fig 3c). Trees are able to carry on transpiring in the dry season due to their deep roots, depleting soil moisture, particularly in the deeper soil layers, whereas grasses cannot. In the 14-year offline spin-up of soil moisture, this produces an increase in initial soil moisture at all four levels under current vegetation compared to 1950s vegetation over the deforested areas. As a result, FSMC is increased (less water stress) by up to 0.1 in some areas. In areas with greater deforestation, even though soil moisture has increased, the trees were able to access more water than the grass that now replaces them, so deforestation causes FSMC to decrease by -0.14 (Fig 3d). In southern areas with coastal deforestation, changes are insignificant because it has been raining in this region for a couple of months and FSMC is high (low water stress for trees and grass).

https://doi.org/10.5194/wcd-2022-49
Preprint. Discussion started: 24 August 2022

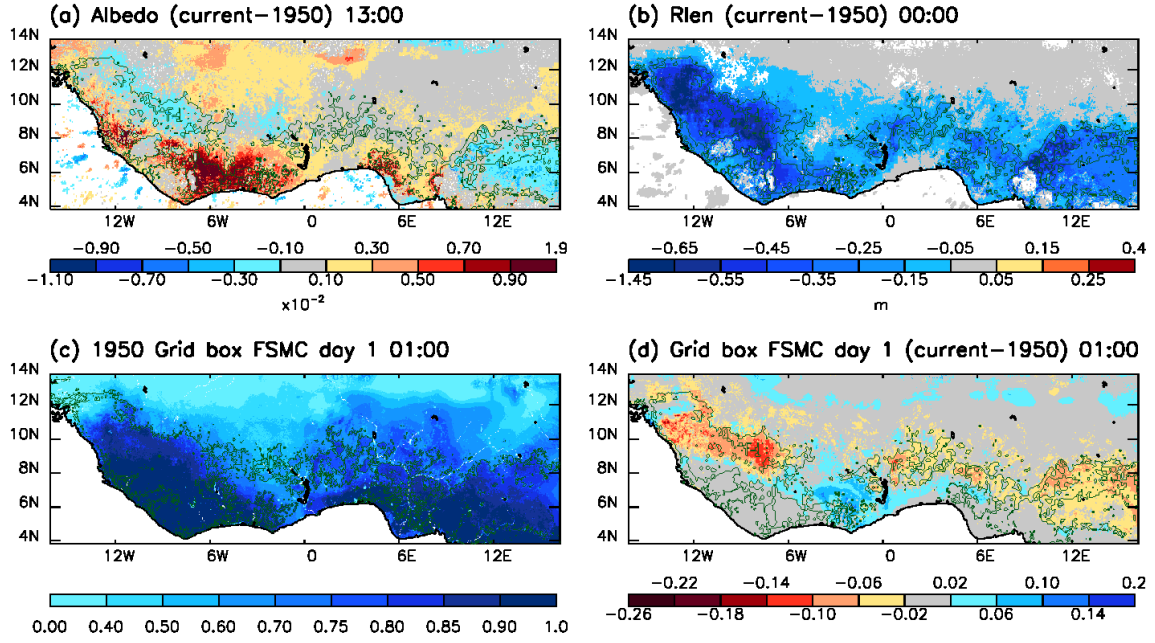

Figure 3: (a) Changes in albedo, (b) Changes in roughness length, (c) 1950s initial FSMC and (d) Changes in initial FSMC. Green contours show where there has been deforestation in (a), (b) and (d) and the 1950s forested region in (c). Insignificant changes are shown in white whereas small but significant changes either side of zero are shown in grey.

3.2 Turbulent and Radiative Fluxes

Diurnal cycles of the change in turbulent and net downward surface radiative fluxes over deforested areas are shown in Fig 4a. Peak differences in radiative and turbulent fluxes occur around 11:00-14:00 UTC. Deforested areas show decreased latent heat flux (LE) throughout the day while sensible heat flux (SH), associated with higher surface temperatures, is increased only until 15:00 UTC. The canopy heat capacity for trees is larger than for grass (areal heat capacities are 320000, 12000 and 8000 J K^{-1} m^{-2} for BT, C4 and C3 grasses respectively). During the morning, more heat is taken to warm the tree canopy than grass, whereas later in the day, the heat stored in the tree canopy is released. Therefore, deforestation causes increases in combined SH+LE in the morning but decreases in the afternoon, when also the maximum in cloudiness and convective activity occurs. In the following, we hence consider pre-convective conditions at 13:00 UTC, when daytime heating is strong and radiative flux differences are maximized.

https://doi.org/10.5194/wcd-2022-49
Preprint. Discussion started: 24 August 2022

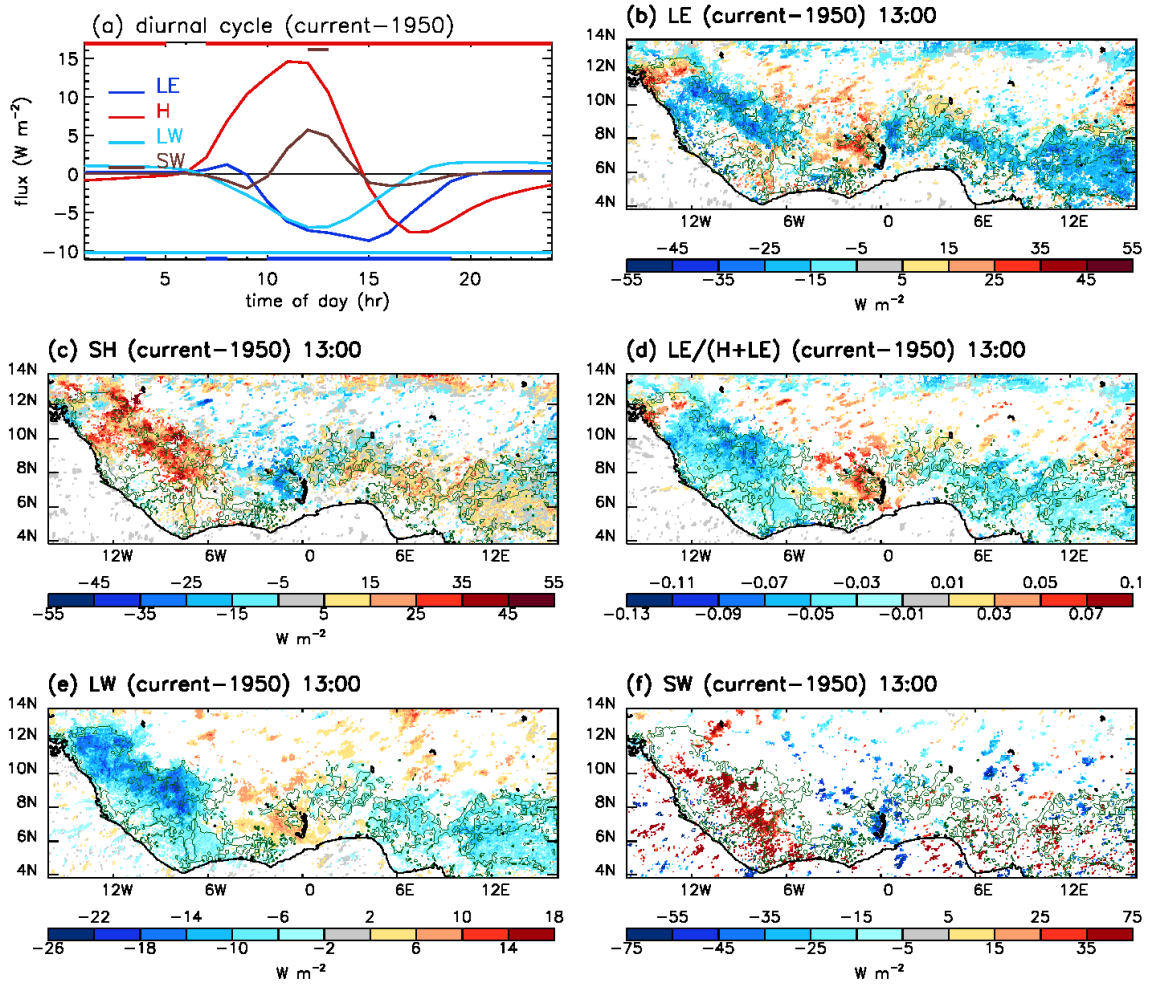

Figure 4: (a) Diurnal cycle of changes in turbulent and radiative heat fluxes averaged over all deforested pixels with times when differences are significant indicated by coloured bars at the top and bottom. Differences in fluxes during the day (13:00 UTC): (b) latent heat, (c) sensible heat, (d) evaporative fraction, (e) net down surface longwave and (f) net down surface shortwave. Insignificant changes are shown in white, whereas small but significant changes either side of zero are shown in grey. Green contours show where there has been deforestation.

Deforested regions predominantly have lower LE (Fig 4b) by up to 30 Wm^{-2}, higher SH (Fig 4c) by up to ~40 Wm^{-2}, and lower evaporative fraction (Fig 4d) at 13:00 UTC. Regions near the coast have insignificant change due to ample soil water here. There are several areas (e.g., around 14° W, 11° N and 3° W, 8° N) where deforestation is accompanied by an increase (rather the expected decrease) in evaporative fraction. This can occur where initial FSMC is increased with current vegetation, as discussed in Section 3.1.

The day-time net downward longwave radiative flux (LW) decreases by up to ~18 Wm^{-2} (i.e., increased emission) due to reduced roughness length suppressing turbulent fluxes and increasing land surface temperature, and a shift in flux partitioning to greater SH and reduced cloud cover both causing near surface temperature to increase (Fig 4e). The net

https://doi.org/10.5194/wcd-2022-49
Preprint. Discussion started: 24 August 2022

downward shortwave radiative flux (SW) is affected by both albedo increases (causes decreases in SW) and by reductions in cloud cover (causes increases in SW) resulting in a patchy overall increase in day-time SW (Fig 4f) by up to ~40 Wm^{-2}. The changes in LW outweigh the changes in SW resulting in a decrease in net radiative flux when averaged over the deforested pixels, but in individual pixels, positive SW changes may dominate, although often the total radiative flux change (not shown) is insignificant.

In summary, averaged across all deforested pixels during the day, the simulations indicate that deforestation increases sensible heat, decreases latent heat and increases long-wave emission. We don't have multi-site long-term flux observations in this region with which to compare the model, but this behaviour is consistent with pan-tropical analyses of increased air temperature responses to deforestation (Alkama and Cescatti, 2016). However, we note that there are deforested regions within the domain where these flux responses are muted (where 1950s soils are wet), or even reversed. Under both these circumstances, the dynamical (roughness) effect is expected to dominate over a negligible thermal effect, as in the simulations of Khanna et al. (2017).

3.3 Near-Surface Temperature and Conditional Instability

Trees shade the surface from the sun during the day, have higher heat capacity and roughness length than grass and transpire more than grass causing evaporative cooling, so we expect land to be cooler in forest regions than grass regions and a warming due to deforestation. At night, the enhanced aerodynamic coupling with the atmosphere that forests exert (compared to smoother surfaces), along with the release of heat absorbed by trees in JULES means that we expect the land to be warmer in forest regions than grass regions, and a cooling due to deforestation. In line with that, Fig 5a shows tropospheric temperature increases during the day up to about 800 hPa and tropospheric temperature decreases during the night up to 900 hPa (with the largest temperature decreases confined to below 950 hPa) when averaged over deforested pixels. Figures 5b and 5c show warmer near-surface temperature during the day (up to 1 K) and cooler near-surface temperature at night (~-0.5 K) in the deforested areas, resulting in a net warming over the whole day. Temperature changes are generally greater where the areal extent of deforestation is greater. Differences also occur outside the deforested areas (e.g., night-time cooling north of the deforestation in Cote d'Ivoire, likely linked to changes in near-surface winds (discussed later), and daytime cooling to the west of Lake Volta due to decreased daytime sensible heat in that location (cf. Fig 4c).

There are significant surface pressure differences (up to 0.3 hPa, not shown) that largely follow the near-surface temperature differences consistent with localized heat-low effects, as discussed by Taylor et al. (2005), but these are more homogeneous across the deforested areas during the day and much patchier at night.

https://doi.org/10.5194/wcd-2022-49
Preprint. Discussion started: 24 August 2022

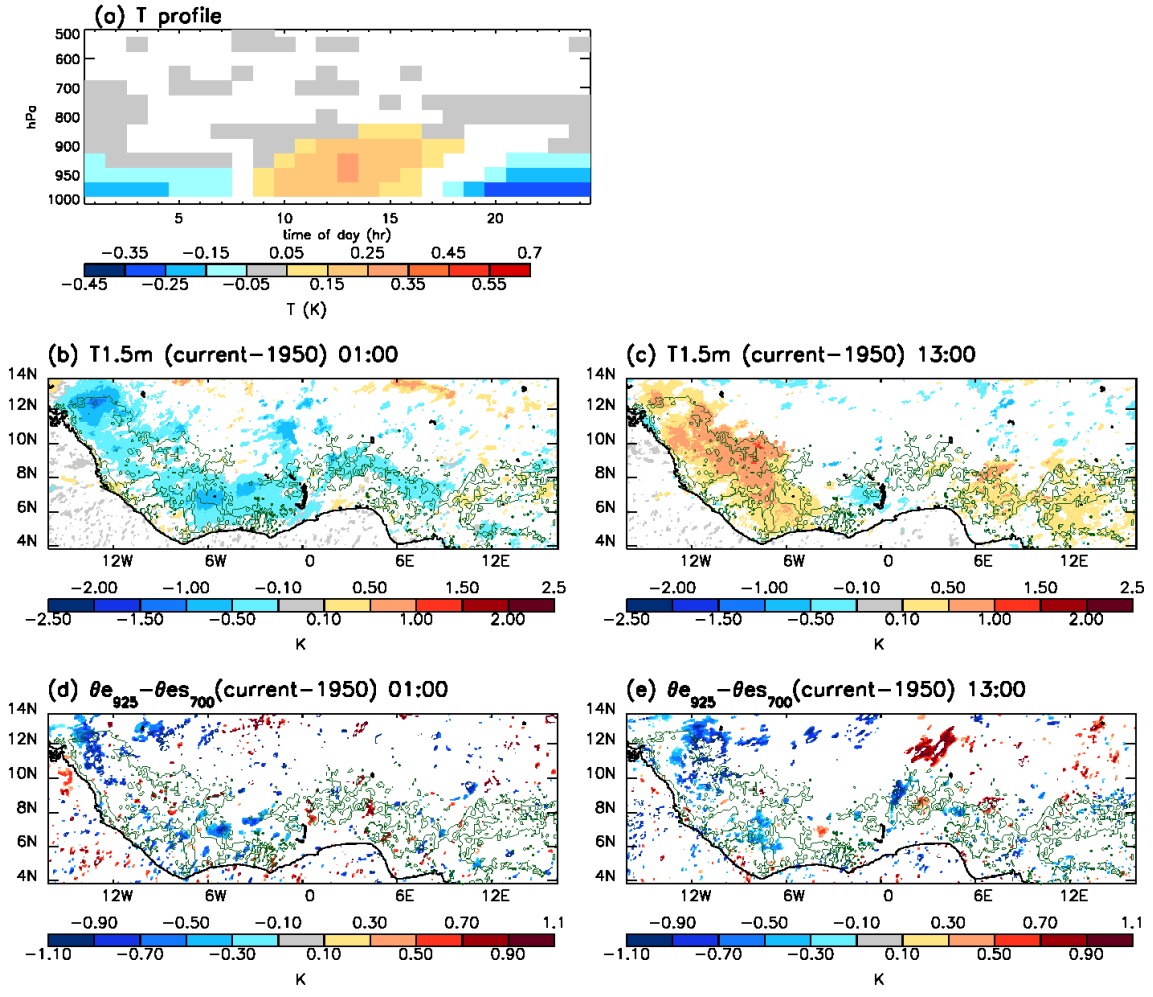

Figure 5: Changes in diagnostics for (a) diurnal cycle of temperature profile averaged over all deforested pixels, and for night (01:00 UTC) (left) and day (13:00 UTC) (right): (b) and (c) near-surface temperature, and (d) and (e) Δθ defined as θ_e at 925 hPa minus θ_{es} at 700 hPa. Insignificant changes are shown in white, whereas small but significant changes either side of zero are shown in grey. Green contours show where there has been deforestation.

We use a 2-level conditional instability measure as a proxy for CAPE: equivalent potential temperature (θ_e) at 925 hPa minus saturated equivalent potential temperature (θ_{es}) at 700 hPa (hereafter called Δθ). Figure 5d and 5e show changes in Δθ. Where lower tropospheric temperature increases during the day, which would increase buoyancy, this is typically coincident with humidity decreases, making the atmosphere less buoyant, resulting in overall decreases in Δθ (by up to 1.1K). In fact, Δθ changes are more related to changes in humidity than changes in temperature (see supplementary Fig S3). The magnitude of changes in Δθ are greater during the day than the night when temperature and humidity changes are less.

https://doi.org/10.5194/wcd-2022-49
Preprint. Discussion started: 24 August 2022

Weather and Climate Dynamics Discussions
Open Access
EGU

3.4 10m Winds

The 1950s 10m winds during night and day are largely south to south-westerly over the region (Fig 6a and 6b). The differences in 10m wind speeds show increases during both day and night over the deforested area (Fig 6c and 6d) as expected due to roughness length decreasing, and the increases are greatest where the 1950s winds are high. There are only small changes in 10m wind direction (Fig 6e and 6f). The changes in 10m winds depend strongly on location and extend into non-deforested regions because there have been small amounts of vegetation change here (see Fig 3b for changes in roughness length) and increases also occur just downwind of the deforestation boundary.

Changes in pressure gradients can also modify the winds by increasing the wind into (deforested) low pressure regions and out of high-pressure regions although this appears to be a weaker effect compared to the roughness length changes. As pressure changes are less at night (mostly insignificant and less than 0.3 hPa) the changes in winds are largely due to the reduced roughness length (night-time changes in winds strongly correlate with expected roughness length scaling, see supplementary Fig S5). Increases in 10m wind speeds are likely to cause convergence on the downwind side and divergence on the upwind side of deforestation as changes are greater within the deforested area than outside.

https://doi.org/10.5194/wcd-2022-49
Preprint. Discussion started: 24 August 2022

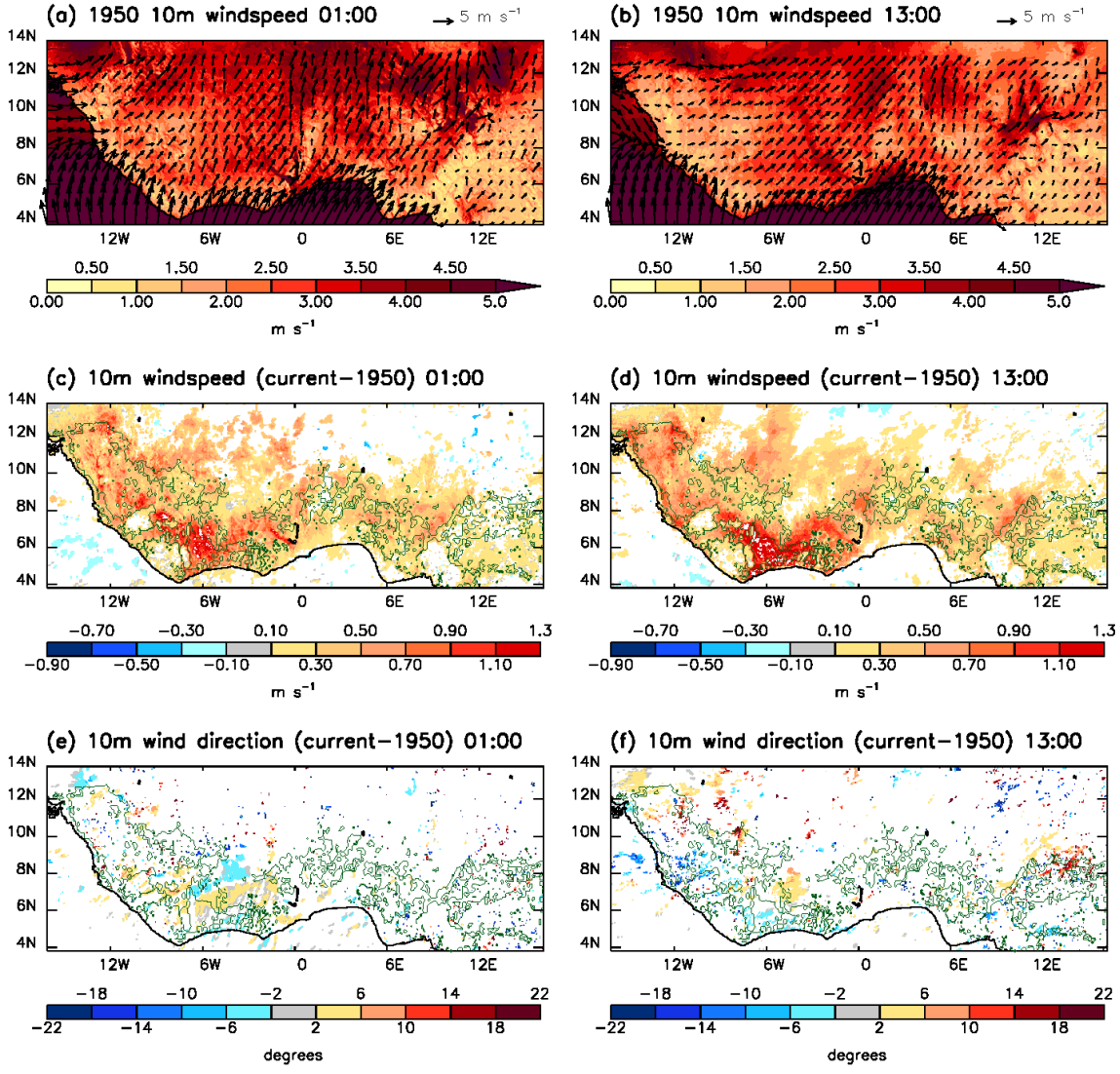

305 **Figure 6: 10m winds for 1:00 UTC (left) and 13:00 UTC (right). 1950 10m wind (speed in shading, direction show by vectors) at (a) 1:00 UTC and (b) 13:00 UTC. Changes in: (a) and (b) 10m wind speed and (c) and (d) 10m wind direction. Insignificant changes are shown in white, whereas small but significant changes either side of zero are shown in grey. Green contours show where there has been deforestation.**

3.5 Rainfall

310 The ensemble-mean daily rainfall accumulation averaged over all land points south of 15° N shows a small but significant increase of +2% (+0.17 mm) in the current vegetation simulations compared to 1950 vegetation simulations (1950=8.35 mm), and this increases to +6% (+0.64 mm) for deforested pixels (1950=10.18 mm) (Fig 7a and 7b). This behaviour is maximized between the hours of 18:00 and 06:00 UTC with an average of +8.4% and a maximum of +12.8% at 00:00 UTC.

https://doi.org/10.5194/wcd-2022-49
Preprint. Discussion started: 24 August 2022

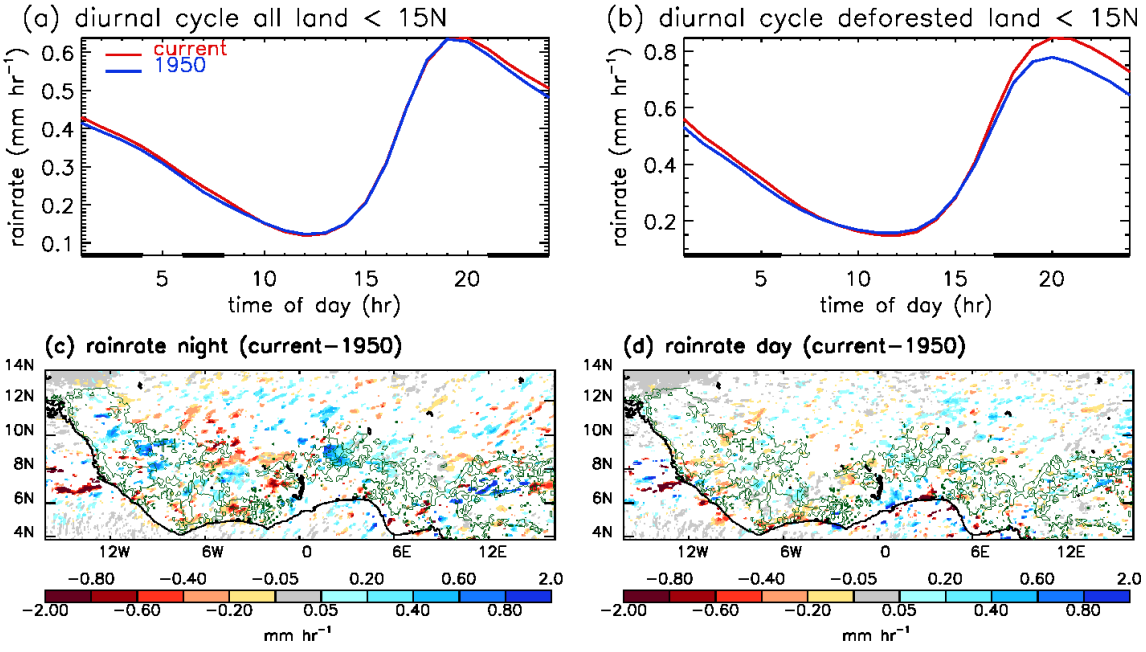

315 **Figure 7: Diurnal cycle of rainfall with times where differences are significant at p=0.1 indicated by black bar for (a) all land points below 15° N and (b) deforested pixels only. Maps of rainfall differences for (c) 19:00-6:00 UTC and (d) 7:00-18:00 UTC. Insignificant changes are shown in white, whereas small but significant changes either side of zero are shown in grey. Green contours show where there has been deforestation.**

Maps of the change in ensemble mean rain rate averaged over the night-time and daytime are presented in Fig 7c and d
320 respectively. This also shows larger and more significant changes at night, with increases over many deforested areas, but also with decreases in some areas and changes also occurring in non-deforested regions (e.g., north Côte d'Ivoire). From this short set of simulations, small scale rainfall changes are too noisy to draw robust conclusions about the nature of the rainfall response to deforestation locally. Aggregated over all deforested areas however, an increase in rainfall with deforestation clearly emerges (Fig 7b), consistent with observations for this region (Taylor et al., 2021).

325 **3.6 Drivers of rainfall change in specific regions**

We now assess in detail the changes in two specific regions (shown in Fig 2g), chosen for their contrasting soil wetness and proximity to the coast. In the first case, the deforestation is up to 400 km from the coast, and the simulation takes place 1-2 months into the rainy season. This means that evapotranspiration is still limited by soil moisture ~200 km or more inland (i.e., FSMC<1) such that deforestation induces a decrease in evaporative fraction and atmospheric warming. In the second
330 region, with marked deforestation 40-200 km from the south coast, the earlier start to the rainy season means that soil moisture is not so limited and has only a minor impact on evaporative fraction during the simulation. Moreover, rainfall in this second case is strongly influenced by the daytime penetration of the sea breeze.

https://doi.org/10.5194/wcd-2022-49
Preprint. Discussion started: 24 August 2022

Mesoscale convective systems (MCSs) produce 56-70% of the rainfall in the sub-Sahelian region of West Africa (Marlon et al., 2018). These storms tend to initiate in the afternoon to early evening and last for many hours. We use a MCS tracking algorithm on 15-minute rain rate fields to find storms where rain rate exceeds 1 mm/hr and where the storm reaches at least 1000 km^2 in area at some point in its lifetime. The algorithm is described in Crook et al (2019). For both regions where we see a significant change in rainfall, we determine frequency and properties of storms within the region over land at each time of the day in both 1950 simulations and current simulations to understand the changes in rainfall. Mostly, the significant changes in rainfall occur in the evening, sometimes reaching into the early hours of the morning.

For both regions, we find that LE decreases for deforested areas but usually only between the hours of 12:00-18:00 UTC. Although this reduced LE would result in less moisture availability during the afternoon, this did not affect the rainfall significantly because most rain falls between 15:00 UTC and the early hours (see Fig 7b) and moisture may be advected more from the coast due to increased onshore winds. We assess diurnal cycles of $\Delta\theta$, specific humidity changes, 1.5m temperature changes, pressure changes and changes in 10m convergence caused by the changes in pressure (see section 3.3) and 10m winds (see section 3.4) to show that how deforestation affects the dynamics and thermodynamics is critical for how the rainfall changes.

3.6.1 Inland Deforestation with Soil Moisture Stress

In this region (Liberia/Sierra Leone/Guinea East, 10-8° W), 1950s rainfall is greatest on the northern half of the 1950s forest (8-10° N) during the afternoon and evening (Fig 8a). 1950s convergence (Fig 8c) is greatest at the coast and positive in locations where the gradient in roughness length (Fig 8b) becomes positive (forest/grass boundaries, at ~7° N, 8.2° N and 9° N). The effect of the sea breeze front (positive convergence) moving inland over the evening from 6- ~7° N is also apparent in Fig 8c. The regions of positive convergence coincide with the high rainfall. This is a region with extensive deforestation 300-400 km inland (deforestation is patchy from 5.5-7.5° N and more extensive from 8-10.5° N) (Fig 8e and h) where the daytime temperature (Fig 8g) and turbulent flux changes are large. There is a significant increase in rain from 16:00 UTC to the early hours of the morning and a significant decrease from 10:00-13:00 UTC at 8-10° N (Fig 8d). There is also a general indication of slightly reduced rainfall south of 8° N. Positive rainfall changes occur where there is generally more convergence (Fig 8f). Negative rainfall changes occur where there is less convergence (south of 8° N) or where specific humidity decreased (e.g., 8-11° N during the day). Changes in convergence (Fig 8f) are affected by changes in roughness length (Fig 8e and h) and changes in pressure (Fig 8g). There is no impact on the sea breeze front because there is very little deforestation and no significant temperature change near the coast. From 7-8° N on the upwind edge of the main deforestation, there are less convergent conditions over much of the day due to roughness length changes to the north. From 10:00-18:00 UTC convergence is also decreased due to pressure decreases to the north. From 9-11° N we would expect more convergent conditions throughout the day due to roughness length changes. Pressure reductions also have an effect north of 8° N from 7:00-23:00 UTC and particularly from 9-11° N between 16:00-20:00 UTC due to the large temperature changes. North of 8° N there are mostly more convergent conditions throughout the whole day. Although LE and therefore low-level

https://doi.org/10.5194/wcd-2022-49
Preprint. Discussion started: 24 August 2022

specific humidity decrease from 8-11° N during the day and are partly responsible for reduced rainfall at this time, the specific humidity increases around 7-10° N in the evening (Fig 8i). The drier air is advected north through the evening with moist air being drawn in from the coast behind it, also resulting in increases in $\Delta\theta$ around 9° N after 20:00 UTC (Fig 8i) (see also supplementary Fig S5).

https://doi.org/10.5194/wcd-2022-49
Preprint. Discussion started: 24 August 2022

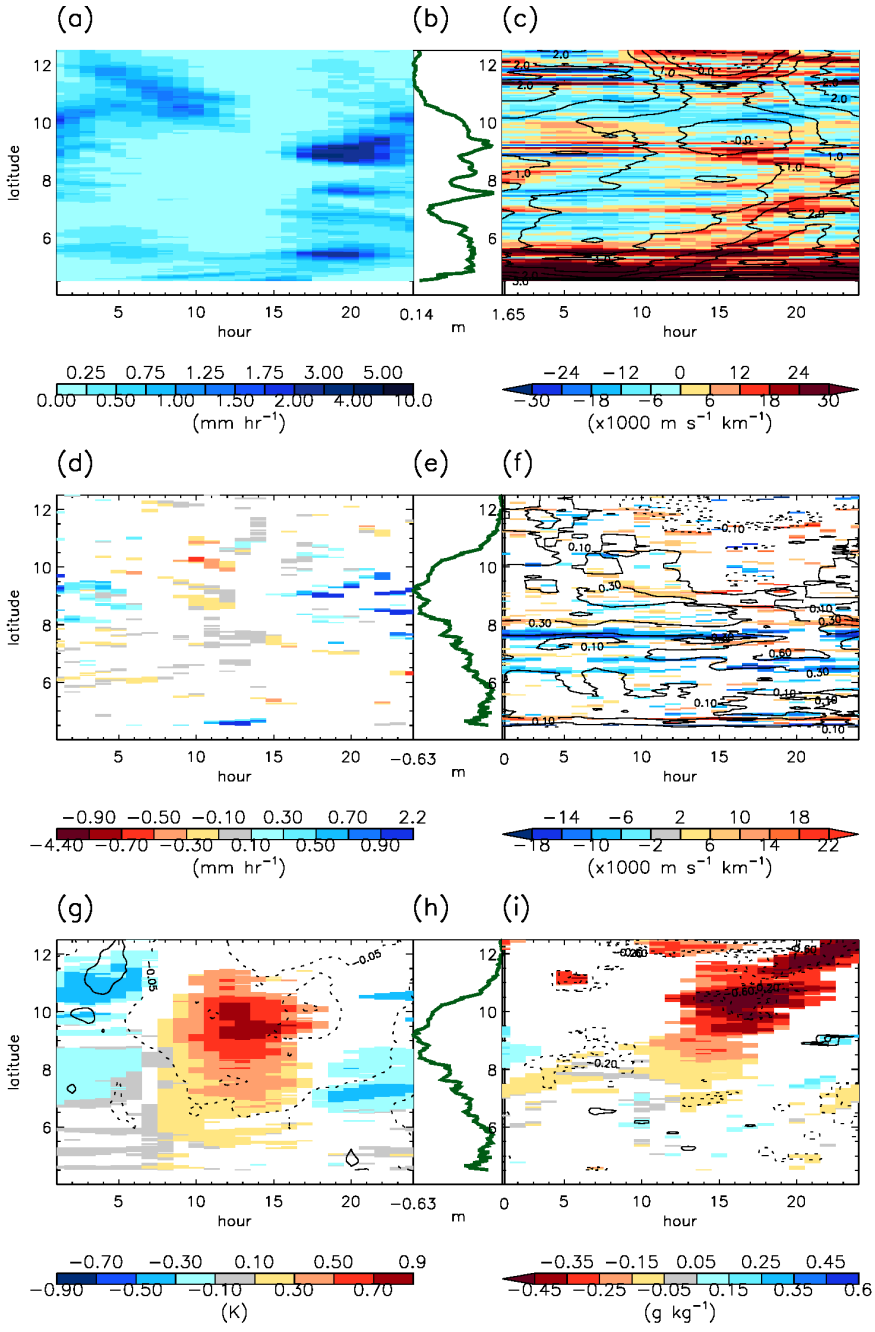

Figure 8: North-south cross sections averaged over 10-8° W over land. Diurnal cycles of (a) 1950s rain rate, (b) 1950s roughness length indicating 1950s forest, (c) 1950s convergence of 10m winds (shading) and 1950s 10m meridional wind (black contours every 0.5 ms^{-1}), changes in (d) rain rate, (e) roughness length indicating the extent of deforestation, (f) convergence of 10m winds (shading) with 10m meridional wind (black contours every 0.2 ms^{-1}), (g) 1.5m temperature (shading) and surface pressure (black contours every 0.1 hPa), (h) roughness length (repeat of (e)), and (i) specific humidity (shading) with Δθ (black contours every 0.4K). Insignificant changes are shown in white, whereas small but significant changes either side of zero are shown in grey.

https://doi.org/10.5194/wcd-2022-49
Preprint. Discussion started: 24 August 2022

Deforestation leads to small increases in the number of initiations in the afternoon and increases in the number of storms throughout the afternoon and evening of ~15% compared to the 1950s and increases of ~40% compared to the 1950s in the early morning in the 8-10° N region (Fig 9a and c). This is consistent with observations in the region (Taylor et al 2022). During the evening, the mean storm area increases by ~20% and into the early hours of the morning before 5:00 UTC, mean storm area and intensity increase by ~30% with increases in area preceding increases in intensity (Fig 9b and c). These all result in higher rainfall. The lower rainfall seen between 8:00-12:00 UTC from 8-10° N is due partly to a smaller number of storms (~25% lower between 8:00-13:00 UTC) but mainly due to the mean storm area being considerably smaller (30-70% between 5:00-14:00 UTC). Note a similar balance of processes is responsible for the enhanced precipitation over a deforested area further west in Guinea.

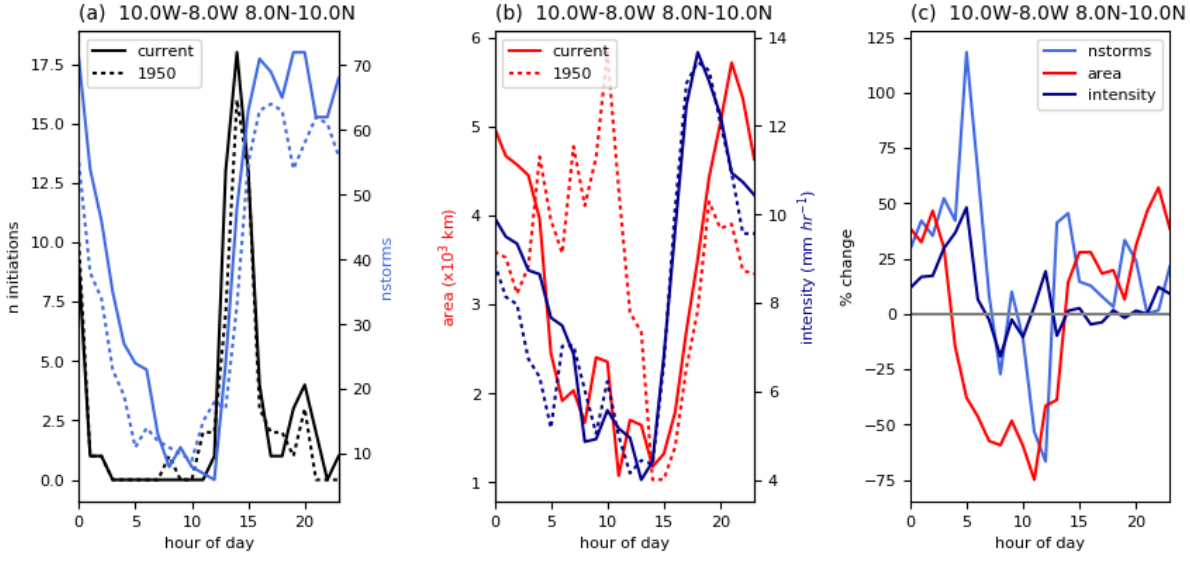

Figure 9: Diurnal cycles in the region 10-8° W, 8-10° N of (a) number of spontaneous initiations and number of storms present, (b) mean area and mean intensity of storms and (c) the % change in number of storms, mean area, and mean intensity.

3.6.2 Coastal deforestation

In this region (Cote d'Ivoire, 6-3° W), 1950s rainfall (Fig 10a) is greatest near the coast over much of the day and driven by the sea breeze. The strong 1950s onshore winds and the sea breeze convergence is a dominant feature (Fig 10c) causing the coastal rain to move inland to 7° N during the evening.

This is an area of near-coastal deforestation (Fig 10e) where the turbulent flux and daytime temperature changes (Fig 10g) are smaller than in the previous region. This region shows two distinct sub regions regarding rainfall responses to deforestation (Fig 10d), caused by a northward shift in rainfall. The rainfall changes follow the changes in convergence (Fig

https://doi.org/10.5194/wcd-2022-49
Preprint. Discussion started: 24 August 2022

10f), i.e., greater convergence results in greater rainfall. There are only small changes in surface pressure (Fig 10g) showing that the changes in convergence (mesoscale circulation changes) are mostly due to roughness length changes, i.e., a dynamical rather than thermal response. Latent heat decreases mostly between 13:00-18:00 UTC from 6-7° N (not shown), resulting in a decrease in low-level (925 hPa) specific humidity (Fig 10i), yet here there is no significant change in coincident rainfall. See also supplementary Fig S7 for specific humidity and wind profiles.

From 5-6.5° N there has been a decrease in rainfall between 14:00-0:00 UTC coincident with a decrease in convergence. This largely coincides with the southern part of the deforestation. We find a reduction in the number of spontaneous initiations in the early afternoon and a reduction in the number of storms (~20%) throughout the day here (Fig 11a and c) as well as a reduction in the mean area (~35%) and intensity (~15%) of storms in the evening (Fig 11b and c). The increase in mean area and intensity of ~15% between 8:00-13:00 UTC does not result in increased rain due to the coincident reduction in the number of storms.

From 6.5-8.0° N there has been an increase in rainfall between 15:00-0:00 UTC. This coincides with the northern edge of deforestation. There are more convergent conditions, from 8:00-0:00 UTC (Fig 10f). Low level specific humidity around 7° N increases from ~18:00 UTC with the band of wetter air moving northward during the evening until it reaches 8° N at 0:00 UTC (Fig 10i) and drier more stable (lower $\Delta\theta$) air follows just to the south. We find more initiations from 12:00-15:00 UTC and more storms (~80% increase) from 13:00-0:00 UTC (Fig 11d and f). We find larger mean area (~60% increase) from 17:00-0:00 UTC and an increase in mean intensity (~20%) from 17:00-22:00 UTC (Fig 11e and f).

https://doi.org/10.5194/wcd-2022-49
Preprint. Discussion started: 24 August 2022

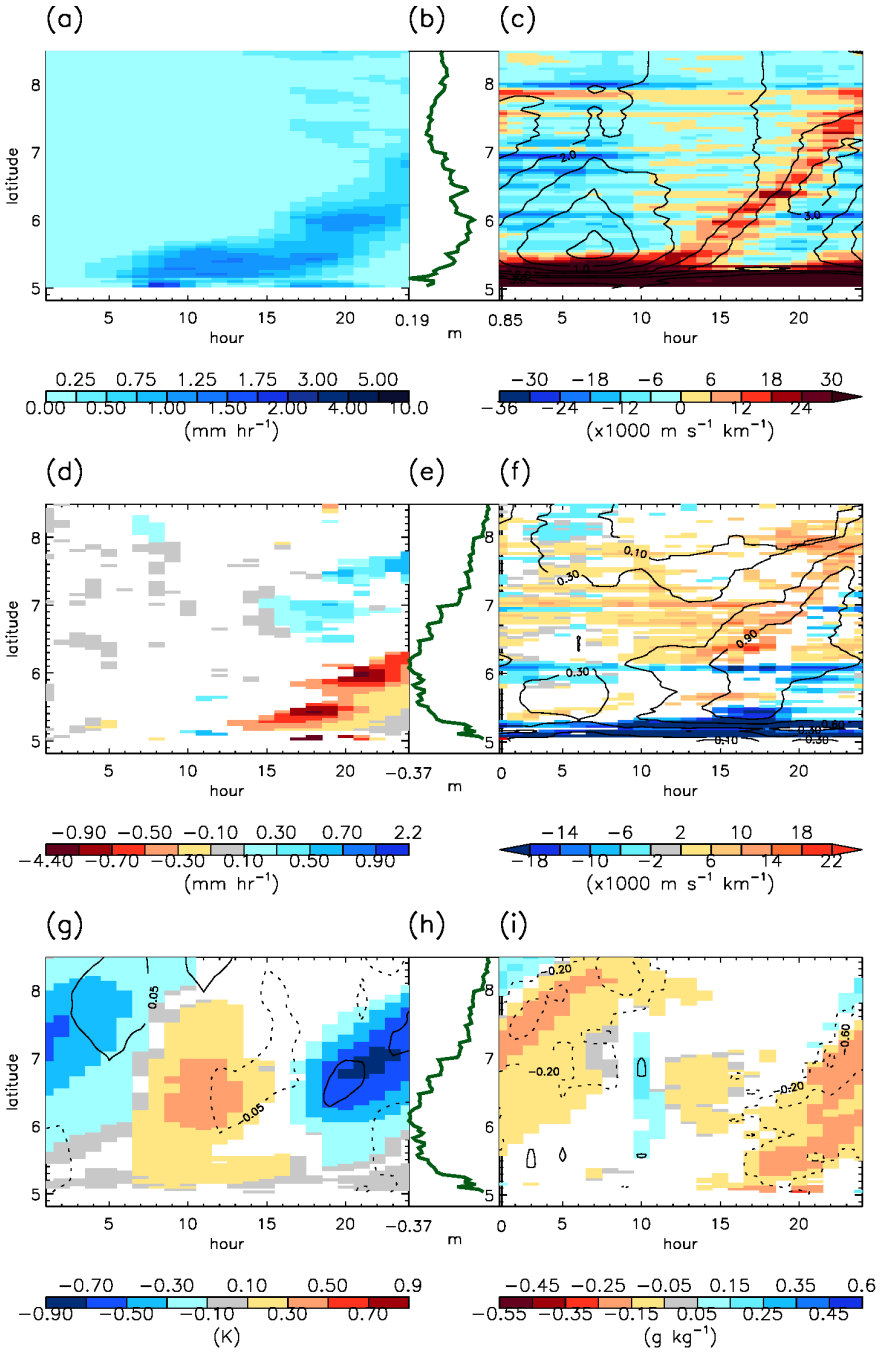

Figure 10: As for Fig 8 but for cross sections 6-3° W.

https://doi.org/10.5194/wcd-2022-49
Preprint. Discussion started: 24 August 2022

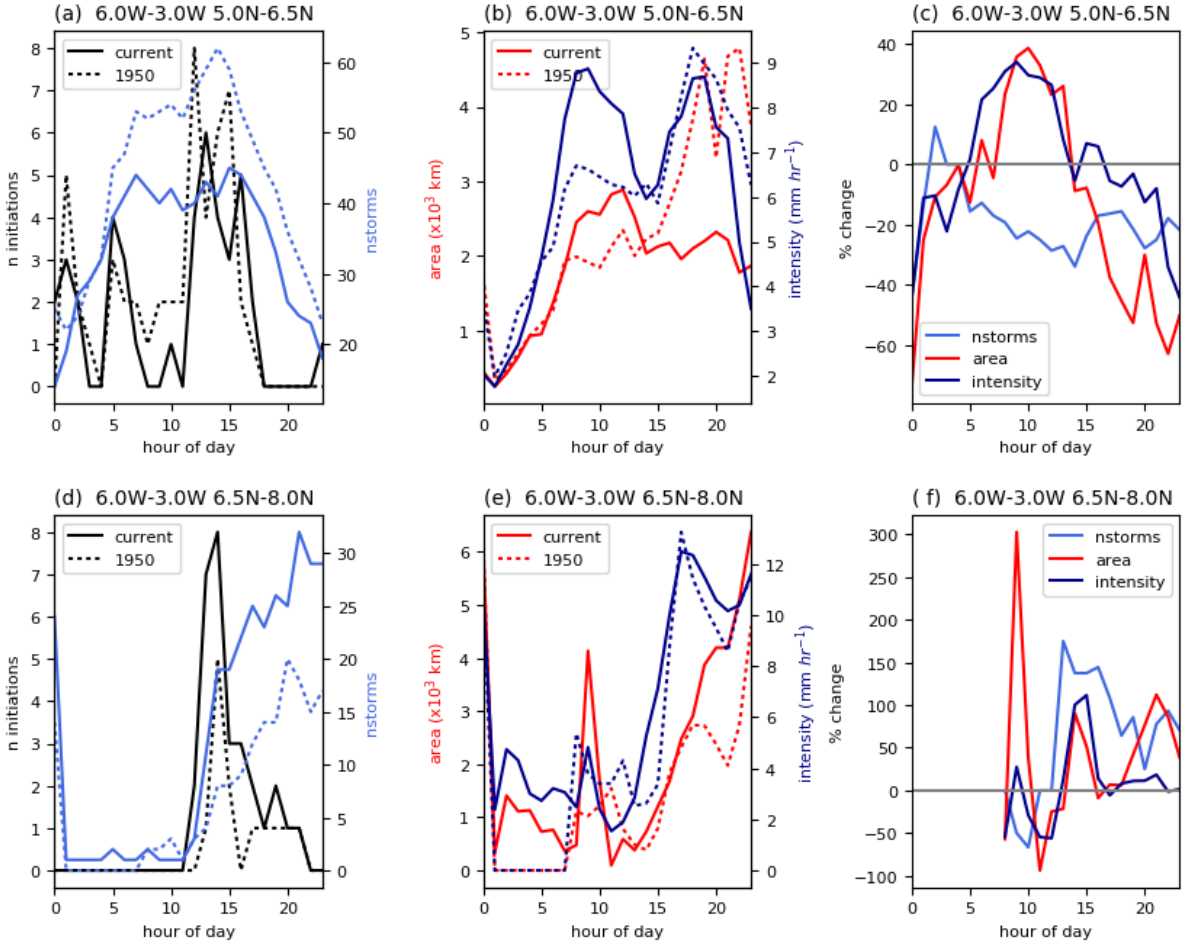

Figure 11: As for Fig 9 but for cross sections 6-3° W and 2 different sub-regions.

In this region, where thermal effects of deforestation are minor, changes in convergence caused by reduced surface roughness drives the sea breeze further inland in the afternoon and evening (see Parker et al. 2017, their Fig 4.18), suppressing convection in the subsiding air behind the sea breeze front and resulting in a shift in rainfall from 5-6.5° N to 6.5-8° N.

4 Comparison with other studies

We now compare our daily mean results over land in the region 16° W-16° E, 0-15° N to three studies which look at the summer season in West Africa with deforestation scenarios of increasing realism, described in Table 1 – Abiodun et al. (2008) (A08), Boone et al. (2016) (B16) and Chilukoti and Xue (2020) (C20). It should be noted that our simulations only

https://doi.org/10.5194/wcd-2022-49
Preprint. Discussion started: 24 August 2022

ran for 5 days in June whereas these studies look at multi-year seasonal changes and therefore are not directly comparable. However, a comparison in terms of the sign of the change is at least worthwhile. We would expect the magnitude of our changes to be less than that seen in other studies due to the less extreme deforestation. Our results suggest that much of the deforested area now has enhanced rainfall, with an average increase of 6% over the whole day over deforested pixels. A08, found decreases over the deforested area of 45% and B16 and C20 found decreases in rainfall over all land of 4-25%, although in B16, half the models showed the rainfall shifting south.

Our imposed deforestation scenario (~11% reduction in trees) translates into local albedo increases of up to 0.02 with a mean of 0.0014, and a mean roughness length decrease of 0.38m. The increases in albedo for some models in B16 are an order of magnitude larger than our albedo increases, although some models had similar albedo changes; in A08 the albedo increased by ~0.1 (45%); in C20 the albedo increase is similar to ours. In A08, roughness length decreased by between 0.25m and 1.95m (based on disturbed forest or tropical forest changing to short grass, see their table 1). The reduced roughness over grass compared to trees has a significant effect on the 10m winds over deforested areas. As generally over West Africa the 10m winds are south westerly, this means both 10m U and V increase. Over the whole day we find V increased by 0.23 ms^{-1}, a similar magnitude to that seen in A08.

We find the net downward LW radiative flux decreases during the day by 3 Wm^{-2} over the deforested area (due to enhanced surface emission) and net downward SW radiative flux changes were more variable but mostly positive. Our whole day mean values (LW = -1.1 Wm^{-2}, SW = +0.3 Wm^{-2}) are the same sign as, albeit an order of magnitude smaller than, A08 and C20. Compared to our simulations, the net downward radiative flux decrease was much greater in some models in B16 due to albedo changes being more dominant in those models than reductions in cloud cover.

We find latent heat flux is generally reduced during the day by 4 Wm^{-2} over deforested areas as is expected, with whole day value of -2.3 Wm^{-2}. We find sensible heat increases during the day by 5 Wm^{-2} with whole day value of +1.3 Wm^{-2}. These are the same sign albeit somewhat smaller than in A08 and C20 and falls within the large range from different models in B16.

Deforested areas are mostly warmer during the day (up to 1 K, deforested mean 0.2K) and cooler during the night (down to -0.5 K, deforested mean -0.2K). Effects are constrained to the lower troposphere (lower than 700 hPa). Temperature changes are usually larger when the extent of the deforestation is larger such as in the west of this region of study. Over the whole day we found no significant change whereas A08, B16 and C20 found up to 1K warming.

Our deforestation scenario is not as extreme in extent or intensity as many previously assessed deforestation scenarios (e.g., A08, B16, C20) and therefore we might not expect the large reductions in rainfall seen previously. A more extreme deforestation scenario may well have greater effect on atmospheric moisture. However, the changes in a number of atmospheric diagnostics are of the same sign and not too dissimilar in magnitude to these other studies, yet we see increases in rainfall.

https://doi.org/10.5194/wcd-2022-49
Preprint. Discussion started: 24 August 2022

	Our study (June)	A08 (JAS)	B16 (JAS)	C20 (JJA)
Deforestation extent	Reduction in trees of 11% in region	100% removal of trees south of 17N	Reduction in trees ~20% in region	Time dependent reduction in trees up to ~30% south of 15° N by 2010
Rain (all land)	+2%	N/A	-4% to -25%	-10%
Rain (deforested land)	+6%	-45%	N/A	N/A
Albedo	+0.0014	+0.1	0 to +0.14	<0.01
Roughness length (m)	-0.38	-0.25 to -1.95	N/A	N/A
LW (Wm^{-2})	-1.1	-10	N/A	-8
SW (Wm^{-2})	+0.3	+5	N/A	+4
LW+SW (Wm^{-2})	-0.8	-5	0 to -30	-4
LE (Wm^{-2})	-2.3	-40	0 to -50	-6
H (Wm^{-2})	1.3	+20	0 to +40	+8
T 1.5m (K)	0	+1	0 to +1	+0.8
V 10m ($m\ s^{-1}$)	0.23	0.5	N/A	N/A

Table 1: Comparison of whole day mean variables over 16W-16E, 0N-15N (deforested land unless specified otherwise), estimated from figures in A08, B16 and C20 if not given as region means.

5 Conclusions

We have assessed the impact of recent deforestation in West Africa on rainfall in early June using an ensemble of 5-day simulations with a CPM. Our deforestation scenario is more realistic and less extreme than previous studies and we assessed the changes over the diurnal cycle. We also assessed the statistics of MCSs. Whilst our simulations examine only a brief period within the full annual cycle, the analysis draws out key processes driving the rainfall response. Our results show much of the deforested area now has enhanced rainfall (mostly due to more storms but also bigger storms and to a lesser degree more intense storms) between 18:00-6:00 UTC, with an average increase of 8.4% across all deforested pixels, and whole day increases of 2% (6%) over all land (deforested land) up to 15° N, unlike previous studies. The changes are more significant during the night than the day and how the rainfall changes is strongly dependent on both soil moisture status and the proximity to the coast of the deforestation due to sea breeze interactions.

We consider two contrasting deforestation areas. In the first case, where the deforested zone is well inland, soil moisture limitation ensures enhanced sensible heat, which creates thermally-driven convergence over the deforested zone. Roughness length induced reductions in convergence to the south and increases in convergence in the north of the deforested zone also

https://doi.org/10.5194/wcd-2022-49
Preprint. Discussion started: 24 August 2022

occur and rainfall increases locally within the deforested zone. However, in the second case, where wetter soils mean there is little impact of deforestation on boundary layer temperatures, reduced roughness lengths are responsible for changes in rainfall. The deforestation maximum lies ~100km from the coastline, and weaker surface drag allows the sea breeze to penetrate faster and further into the interior. The associated changes in convergence and advection of moist oceanic air effectively reduces rainfall near the coast whilst enhancing it inland. Our results show that deforestation near the coast where the sea breeze impacts convection results in very different patterns of rainfall changes than deforestation further inland. A similar conclusion was drawn in the observational study by Taylor et al. (2022). Focusing on deforestation within a coastal strip of 50km, they found enhanced convective activity maximized within that strip, embedded within the sea breeze. The two analyses differ both in the proximity of the deforestation to the coastline, and the likely role of thermal effects. Considering the location in the current study, the deforestation is further inland, and that draws sea breeze convection away from the coastal strip. Secondly, whilst the model analysis focuses on a location and time of year when soil moisture effects are less important, the observational analysis draws from a broader range of conditions in space and time, and thermal effects are expected to be more important.

We have shown that changes in low level winds over deforested areas can cause more convergent conditions into the evening when MCSs are numerous. Although humidity (and conditional instability) does decrease over deforested areas in the day, it recovers in the evening and can increase in some areas due to enhanced advection inland due to increased winds. However, the changes in convergence in our model were found to be the dominant control on rainfall with little impact from changes in the moisture budget, in line with observed rainfall changes in the region (Taylor et al 2022) and with observed increases in cloud cover over deforested regions in general in the tropics (Xu et al. 2022). We also find that changes are quite localized, and we did not see many significant changes in any variable north of 15° N. The African Easterly Jet also did not change position in our model, but this has been found to occur in other studies (B16). However, our simulations are over a short time. Our model adds strong support to the observationally-based link between deforestation and increased rainfall in the coastal zone (Taylor et al., 2022). Our results illuminate the mechanisms responsible and demonstrate that the processes at work differ from region to region according to the precise geographic environment (i.e. distance from coast) and seasonally (according to overall water stress).

In contrast to PMs, CPMs show enhanced rainfall in areas where there is mesoscale convergence (Birch et al 2014), for example along soil moisture boundaries, in line with observed mechanisms (Taylor et al., 2013), rather than being controlled by the moisture budget. It has also been found that CPMs better capture the rainfall response to sea breeze changes (Finney et al., 2020). PMs simulate the convective peak too early in the day (~13:00 UTC) compared to observations and CPMs. Such models would be more affected by the reduced evaporation caused by deforestation during the early afternoon, as rainfall is strongly controlled by the vertical profile of temperature and moisture, which could explain why previous deforestation studies show a tendency to reductions in rainfall over deforested areas. Therefore, we suggest that the mesoscale convergence produced by deforestation is likely to affect rainfall more than previously found in studies using PMs. It is imperative that further studies using CPMs over extended periods are undertaken to understand whether our

https://doi.org/10.5194/wcd-2022-49
Preprint. Discussion started: 24 August 2022

findings are representative of all CPMs. We have demonstrated that a CPM can capture the effects of enhanced convergence due to deforestation and in principle could be used to make future projections of changes due to deforestation. However, substantial time was taken initially to improve the land surface model and the surface conditions, and we would not expect such projections yet to be reliable without a comparable effort to ensure that the model setup is good enough (out-of-the-box models have very different representations of land cover and bio-geophysical responses e.g., Pitman et al., 2009, and Boone et al., 2016).

Code/Data availability

Model output is available at Crook, J. (2021): VERA: West Africa current vegetation and 1950 vegetation scenario ensemble mean data for June 2014. Centre for Environmental Data Analysis, https://catalogue.ceda.ac.uk/uuid/db259fd2bad64b6da9af884121a160a6.

Author contributions

Julia Crook performed the model simulations, analyzed the simulation outputs, wrote the manuscript, and curated the data.
Cornelia Klein contributed to reviewing and editing the manuscript.
Sonja Folwell developed the 1950s vegetation map, produced the ancillaries required for the simulations, made the modifications required to JULES and contributed to writing the manuscript.
Chris Taylor and Doug Parker acquired funding, performed project administration, and contributed to reviewing and editing the manuscript. Chris Taylor also had significant input into understanding issues with the standard UM model setup.
Adama Bamba and Kouakou Kouadio helped in the analysis of the sea breeze impacts in the Cote d'Ivoire region.

Competing interests

The authors declare that they have no conflict of interest.

Acknowledgments

This work used the ARCHER UK National Supercomputing Service (http://www.archer.ac.uk) to run the simulations. We thank Willie McGinty (National Centre for Atmospheric Science) for help in setting up the simulations. The work was funded by Natural Environment Research Council (NERC) VERA project (NE/M003574/1) and NERC/DFID AMMA-2050 project (NE/M020126/1). Parker was supported by a Royal Society Wolfson Research Merit Award (2014-2018).

https://doi.org/10.5194/wcd-2022-49
Preprint. Discussion started: 24 August 2022

References

Abiodun, B., Pal, J. S., Afiesimama, E., Gutowski, W. & Adedoyin, A: Simulation of West African monsoon using RegCM3 Part II: impacts of deforestation and desertification, Theor. Appl. Climatol. 93, 245–261, 2008.

Aleman J.C., Jarzyna M.A., & Staver A.C.: Forest extent and deforestation in tropical Africa since 1900, Nature Ecology & Evolution 2(1):26-33, 2018.

Alkama, R. and Cescatti, A.: Biophysical climate impacts of recent changes in global forest cover, Science 351 6273, pp. 600-604, 2016.

Best, M. J. et al.: The Joint UK Land Environment Simulator (JULES), model description – Part 1: Energy and water fluxes, Geosci. Model Dev., 4(3), 677–699, doi:10.5194/gmd-4-677-2011, 2011.

Birch, C. E., Marsham, J. H., Parker, D. J., and Taylor, C. M.: The scale dependence and structure of convergence fields preceding the initiation of deep convection, Geophys. Res. Lett., 41, 4769–4776, doi:10.1002/2014GL060493, 2014

Boone, A.A., Xue, Y., De Sales, F. et al.: The regional impact of Land-Use Land-cover Change (LULCC) over West Africa from an ensemble of global climate models under the auspices of the WAMME2 project, Clim Dyn 47, 3547–3573, https://doi.org/10.1007/s00382-016-3252-y, 2016.

Brandt M., et al.: Human population growth offsets climate-driven increase in woody vegetation in sub-Saharan Africa, Nature Ecology & Evolution 1:0081, 2017.

Chagnon, F.J.F. & Bras, R.L: Contemporary climate change in the Amazon, Geophys. Res. Lett. 32, L13703, 2005.

Chilukoti, N, and Xue. Y.: An assessment of potential climate impact during 1948–2010 using historical land use land cover change maps, Int. J. Climatol. 41:295–315, DOI 10.1002/joc.6621, 2020.

Crook, J., Klein, C., Folwell, S., Taylor, C. M., Parker, D. J., Stratton, R., and Stein, T.: Assessment of the representation of West African storm lifecycles in convection-permitting simulations. Earth and Space Science, 6, 818–835. DOI: 10.1029/2018EA000491, 2019.

D'Almeida, C., Vorosmarty C.J., Hurtt, G.C., Marengo, J.A., Dingman, S.L., and Keim, B.D.: The effects of deforestation on the hydrological cycle in Amazonia: a review on scale and resolution, Int. J. Climatol.27:633–647. DOI: 10.1002/joc.1475, 2007.

Dee, D. P., Uppala, S. M., Simmons, A. J., Berrisford, P., Poli, P., Kobayashi, S., et al.: The ERA-Interim reanalysis: configuration and performance of the data assimilation system, Q.J.R. Meteorol. Soc., 137: 553–597. doi:10.1002/qj.828, 2011.

Duveiller, G., Hooker, J, and Cescatti, A.: The mark of vegetation change on Earth's surface energy balance, Nature Communications, 9:679. doi:10.1038/s41467-017-02810-8, 2018.

Finney, D. L., Marsham, J. H., Rowell, D. P., Kendon, E. J., Tucker, S. O., Stratton, R. A., and Jackson, L. S.: Effects of Explicit Convection on Future Projections of Mesoscale Circulations, Rainfall, and Rainfall Extremes over Eastern Africa, J. Climate, 33(7), 2701-2718. doi 10.1175/JCLI-D-19-0328.1, 2020.

https://doi.org/10.5194/wcd-2022-49
Preprint. Discussion started: 24 August 2022

Funk, C., Peterson, P., Landsfeld, M., Pedreros, D., Verdin, J., Shukla, S., . . . Michaelsen, J.: The climate hazards infrared precipitation with stations-a new environmental record for monitoring extremes, Scientific Data, 2. DOI:Artn 150066 10.1038/Sdata.2015.66, 2015.

Garcia-Carreras, L. and Parker, D. J.: How does local tropical deforestation affect rainfall?, Geophys. Res. Lett. 38, L19802, DOI:10.1029/2011gl049099, 2011.

Garcia-Carreras, L., Parker, D.J., and Marsham, J.: What is the mechanism for the modification of convective cloud distributions by land surface-induced flows?, J. Atmos. Sci., 68, 619–634, 2011.

Hartley, A. J., Parker, D.J., Garcia-Carreras, L., Webster, S.: Simulation of vegetation feedbacks on local and regional scale precipitation in West Africa, Agricultural and Forest Meteorology, 222, p59-70, doi.org/10.1016/j.agrformet.2016.03.001, 2016.

Hurtt, G. C., Chini, L. P., Frolking, S., Betts, R. A., Feddema, J., Fischer, G., and Wang, Y. P.: Harmonization of land-use scenarios for the period 1500-2100: 600 years of global gridded annual land-use transitions, wood harvest, and resulting secondary lands. Climatic Change, 109(1-2), 117-161, 2011.

Khanna, J., Medivgy, D., Fueglistaler, S. and Walko, R.: Regional dry-season climate changes due to three decades of Amazonian deforestation, Nature Clim Change 7, 200–204. https://doi.org/10.1038/nclimate3226, 2017.

Lawrence, D., and Vandecar, K.: Effects of tropical deforestation on climate and agriculture, Nature Clim. Change 5, 27-36, DOI:10.1038/nclimate2430, 2015.

Marlon, M. Fink, A.H., and Knippertz, P.: Rainfall Types over Southern West Africa: Objective Identification, Climatology and Synoptic Environment, Q. J. R. Met. Soc. doi:10.1002/qj.3345, 2018.

Medvigy, D., Walko, R. L., and Avissar, R.: Effects of Deforestation on Spatiotemporal Distributions of Precipitation in South America, J. Climate, 24, 2147–2163, DOI: 10.1175/2010JCLI3882.1, 2011.

Parker, D.J., Kassimou, A., Orji, B.N., Osika, D.P., Hamza, I., Diop-Kane, M., Fink, A., Galvin, J., Guichard, F., Lamptey, B.L., Hamidou, H., van der Linden, R., Redl, R., Lebel, T.: Local Weather. In: Parker, D.J.; Diop-Kane, M. (eds.) Meteorology of Tropical West Africa: The Forecasters' Handbook. Chichester, UK.: John Wiley & Sons, Ltd, pp. 130-174. https://doi.org/10.1002/9781118391297.ch4, 2017.

Penga, S., Piaoa, S., Zenga, Z., Ciaisc, P., Zhoud, L., Lie, L., Mynenif, R., Yina, Y., and Zengg, H.: Afforestation in China cools local land surface temperature, PNAS, 111 (8) 2915–2919, Doi: 10.1073/pnas.1315126111, 2014.

Perugini, L., Caporaso, L, Marconi, S., Cescatti, A., Quesada, B., de Noblet-Ducoudré, N,. House, J., and Arneth, A.: Biophysical effects on temperature and precipitation due to land cover change, Environ. Res. Lett. 12, 053002. Doi: /10.1088/1748-9326/aa6b3f, 2017.

Pitman, A.J., et al.: Uncertainties in climate responses to past land cover change: First results from the LUCID intercomparison study, Geophys. Res. Lett., 36(14): p. L14814, 2009.

https://doi.org/10.5194/wcd-2022-49
Preprint. Discussion started: 24 August 2022

Poulter, B., MacBean, N., Hartley, A., Khlystova, I., Arino, O., Betts, R., . . . Peylin, P.: Plant functional type classification for earth system models: results from the European Space Agency's Land Cover Climate Change Initiative, Geoscientific Model Development, 8(7), 2315-2328, 2015.

Semazzi, F. H. M. and Song, Y.: A GCM study of climate change induced by deforestation in Africa, Clim. Res. 17, 169–182, 2001.

Semeena, V.S.; Taylor, C.M.; Folwell, S.S., and Hartley, A.: Global gridded monthly mean Leaf Area Index (LAI) for five Plant Functional Types (PFTs) derived from the Global LAnd Surface Satellite (GLASS) products for the period 2000-2014. NERC Environmental Information Data Centre. https://doi.org/10.5285/6d07d60a-4cb9-44e4-be39-89ea40365236, 2021

Silvério, D., Brando, P., Macedo, M., Beck, P, Bustamante, M. and Coe, M.: Agricultural expansion dominates climate changes in southeastern Amazonia: the overlooked non-GHG forcing, Environ. Res. Lett. 10, 104015. doi:10.1088/1748-9326/10/10/104015, 2015.

Souza, E. P., Renno, N. O. and Silva Dias, M. A. F.: Convective circulations induced by surface heterogeneities, J. Atmos. Sci. 57, 2915–2922, 2000.

Spracklen, D.V., Baker, J.C.A., Garcia-Carrera,s L., and Marsham, J.H.: The Effects of Tropical Vegetation On Rainfall. Annual Review of Environment and Resources. 43, pp. 193-218, doi.org/10.1146/annurev-environ-102017-030136, 2018.

Taylor, C.M., Birch, C.E., Parker, D.J., Dixon, N., Guichard, F., Nikulin, G., and Lister, G.M.S.: Modeling soil moisture-precipitation feedback in the Sahel: Importance of spatial scale versus convective parameterization, Geophys. Res. Lett., 40, 6213–6218, doi:10.1002/2013GL058511, 2013.

Taylor, C.M., Klein, C., Parker, D.J., Gerard, F., Semeena, V.S., Barton, E.J., Harris, B.L.: "Late-stage" deforestation enhances storm trends in coastal West Africa. Proceedings of the National Academy of Sciences of USA. 119(2). e2109285119. https://doi.org/10.1073/pnas.2109285119, 2022.

Taylor, C.M., Parker, D.J., Lloyd, C.R., Thorncroft, C.D.: Observations of synoptic-scale land surface variability and its coupling with the atmosphere, Q. J. R. Meterol Soc., 131(607), pp. 913-937, 2005.

UNEP-WCMC and IUCN: Protected Planet: The World Database on Protected Areas (WDPA)/OECM Database [On-line], Downloaded October 2014, Cambridge, UK: UNEP-WCMC and IUCN. Available at: www.protectedplanet.net, 2014.

Vanden Broucke, S., Van Lipzig, N.: Do convection-permitting models improve the representation of the impact of LUC?, Clim Dyn 49, 2749–2763, DOI:10.1007/s00382-016-3489-5, 2017.

Van den Hoof, C., et al.: Improved evaporative flux partitioning and carbon flux in the land surface model JULES: Impact on the simulation of land surface processes in temperate Europe, Agricultural and Forest Meteorology, 181(0): p. 108-124, 2013.

Wang, G., Eltahir, E.A.B., Foley, J.A. et al.: Decadal variability of rainfall in the Sahel: results from the coupled GENESIS-IBIS atmosphere-biosphere model, Climate Dynamics 22, 625–637, DOI:10.1007/s00382-004-0411- 3, 2004.

Werth, D. and Avissar, R.: The local and global effects of African deforestation, Geophys. Res. Lett., 32, L12704, 2005.

https://doi.org/10.5194/wcd-2022-49
Preprint. Discussion started: 24 August 2022

Xiao, Z.Q., Liang, S.L., Wang, J.D., Xiang, Y., Zhao, X. and Song, J.L.: Long-Time-Series Global Land Surface Satellite Leaf Area Index Product Derived From MODIS and AVHRR Surface Reflectance, IEEE TRANSACTIONS ON GEOSCIENCE AND REMOTE SENSING, 54(9), 5301-5318, 2016.

Xu, R., Li, Y., Teuling, A.J. et al.: Contrasting impacts of forests on cloud cover based on satellite observations, Nat Commun 13, 670, https://doi.org/10.1038/s41467-022-28161-7, 2022.

Zheng, X., and Eltahir, E.: The role of vegetation in the dynamics of West African monsoons, J. Clim., 11, 2078–2096, 1998.